Marine Geology 434 (2021) 106419

Contents lists available at ScienceDirect

Marine Geology

journal homepage: www.elsevier.com/locate/margo

Noble gases in sediment pore water yield insights into hydrothermal fluid transport in the northern Guaymas Basin

E. Horstmann [a,b,*], Y. Tomonaga [a], M.S. Brennwald [a], M. Schmidt [c], V. Liebetrau [c], R. Kipfer [a,b]

[a] Eawag, Department of Water Resources and Drinking Water, Überlandstrasse 133, 8600 Dübendorf, Switzerland
[b] ETH Zürich, Department of Environmental System Science, Universitätsstrasse 16, 8092 Zürich, Switzerland
[c] GEOMAR Helmholtz Centre for Ocean Research Kiel, Marine Geosystems, Wischhofstr. 1-3, 24148 Kiel, Germany

ARTICLE INFO

Keywords:
Noble gases
Hydrothermal vents
Black smokers
Guaymas basin
Fluid transport

ABSTRACT

We present noble gas concentrations determined in pore water of deep-sea sediments close to a recently discovered hydrothermal vent site, consisting of a mound structure and several black smokers, located in the northern Guaymas Basin, Gulf of California. Noble gases were used as tracers to identify the origin of fluids within the sediment pore space and to gain insight into transport dynamics of hydrothermal fluids in this region. Our data suggest that Guaymas Basin bottom water is the only source of pore water in the pelagic sediment body close to the hydrothermal vent field. In particular, there is no evidence of any direct (diffusive or advective) transport of hydrothermal fluids through the deep-sea sediments surrounding the black smoker system. This finding implies that at this black smoker site hydrothermal fluids are transported upwards from the fluid source in very narrow pathways below the smokers. Thus, the fluids are only injected into the ocean directly through the chimneys of the black smokers and no additional emission from the surrounding sediment takes place. Helium isotope data show that during a more active phase of the vent field in the past (supposedly representing the early onset of the black smokers 5–6 kyrs ago), bottom water with a different isotopic signature was incorporated into the sediment column.

1. Introduction

First evidence for hydrothermal venting along ocean ridges and ocean floor spreading centers was found in the 1970s (e.g. Talwani et al., 1971; Corliss et al., 1979). Despite extensive research, many concepts of hydrothermal fluid evolution and fluid transport dynamics at spreading centers remain elusive. Moreover, hydrothermally-induced alteration of ocean sediments covering young rifting or spreading zones has the potential to release massive amounts of carbon to the atmosphere during short time periods; this could trigger events like the Paleocene-Eocene Thermal Maximum (Svensen et al., 2004; Berndt et al., 2016), making the understanding of hydrothermal fluid sources and transport mechanisms even more crucial in the context of global warming events.

The Guaymas Basin in the Gulf of California (Fig. 1), a rift basin at the northern extension of the East Pacific Rise (EPR), is such an evolving ocean floor spreading center (Rona, 1984), characterized by the formation of new oceanic crust by upwelling of mantle material into a sedimentary cover.

At the EPR, the formation of black smokers is a typical result of hydrothermal activity. Fluids with temperatures of over 330 °C rise up to the ocean floor and are released through narrow chimneys (Tivey, 2007). The common model of chimney formation for black smokers states that mineral deposits start to precipitate when the hot fluids are injected into the cold ocean water, forming an initial chimney-shaped barrier at the sediment surface (Haymon, 1983; Goldfarb et al., 1983). While minerals precipitate in the pore space of the chimney walls, they become less permeable with time, until fluids are solely ejected at the top (Tivey, 2007). Thus, according to this model, black smoker chimneys can be regarded as impermeable barriers against lateral fluid transport. However, the model only explains what happens directly at the sediment surface at the site of a chimney. It does not explain how fluid transport between the hydrothermal source (at several hundred meters depth) and the sediment surface takes place at a vent site, i.e. whether hydrothermal fluids rise up only along narrow vertical pathways through the pelagic sediment body below the chimney structures, or whether there might also be a part of the fluids which is transported upwards along more widespread (lateral) pathways from the source to the sediment surface. For the latter case, one would expect hydrothermal fluids to emanate

* Corresponding author at: Eawag, Department of Water Resources and Drinking Water, Überlandstrasse 133, 8600 Dübendorf, Switzerland.
E-mail address: edith.horstmann@eawag.ch (E. Horstmann).

https://doi.org/10.1016/j.margeo.2021.106419
Received 2 December 2020; Accepted 4 January 2021
Available online 15 January 2021

diffusely from the sediments surrounding the vent structures as well.

In this study, we present noble gas (NG) data from pore fluids of a sediment core taken close to a hydrothermal vent site in the Northern Trough of the Guaymas Basin, Gulf of California, to identify the geochemical origin of hydrothermal fluids in pelagic sediments and identify transport mechanisms. The active hydrothermal vent field consisting of black smoker chimneys on a mound structure was recently discovered by Berndt et al. (2016) during an expedition in the Guaymas Basin (see cruise report RV SO241: Berndt et al., 2015).

Concentrations of atmospheric noble gases (Ne, Ar, Kr, Xe) in pore water are generally controlled by the physical conditions prevailing in the overlying water body, while He can be used to identify a terrigenic (i.e. mantle or crust derived) fluid component. Ne – Xe enter the ocean through air-water partitioning, so their concentrations are usually found to agree with the atmospheric equilibrium concentration and are only dependent on in-situ ocean water temperature, salinity, and atmospheric pressure (see Kipfer et al., 2002; Brennwald et al., 2013). The same concentrations can be found in sediment pore water of an open water body, since during sedimentation the overlying water is incorporated into the sediment column (Brennwald et al., 2003; Strassmann et al., 2005). Noble gas concentrations in hot hydrothermal fluids, which were subject to subsurface boiling, however, have been found to be depleted by 20 to 30% compared to in-situ conditions (Winckler et al., 2000).

It is possible for NG concentrations to be archived in sediments for a very long time, as diffusion can be heavily suppressed: Studies of NG concentrations in ocean and lacustrine sediments have shown that even in these slightly compacted sediments, the diffusive transport of noble gases in the sediment pore space can be attenuated by several orders of magnitude compared to diffusion in open water; under such conditions, NG concentrations can be preserved over unexpectedly large timescales in the sediment column (Brennwald et al., 2013; Tomonaga et al., 2014; Tomonaga et al., 2015). Brennwald et al. (2013) suggest several reasons and mechanisms for this strong suppression of diffusive transport: (1) A significantly decreased sediment pore size due to a geometric realignment of minerals during sedimentation and compaction (Horseman et al., 1996) which leads to a decrease in viscosity in the pore space ('Renkin effect', see e.g. Renkin, 1954; Grathwohl, 1998; Schwarzenbach et al., 2003; Brennwald et al., 2003), (2) a disconnection of some pores from the otherwise interconnected main pore space (Grathwohl, 1998), (3) the presence of microscopic gas bubbles to which noble gases escape due to their low solubility in water (Winckler et al., 2000), (4) the adsorption of gases onto the sediment matrix (Pitre and Pinti, 2010).

The NG signal in the pore water of surface sediment is usually decoupled from the corresponding sediment during compaction ('compaction flux', Imboden, 1975; Strassmann et al., 2005). Since pore fluids, as opposed to the sediment matrix, are not compacted, fluids which were initially incorporated in a sediment layer will move upwards with time relative to this layer.

Hydrothermal vent fluids are expected to be enriched in He compared to air-saturated water (ASW) since they originate from a mantle derived source, which is a reservoir of isotopically light He (Mamyrin and Tolstikhin, 1984). Mid-Ocean Ridges represent ocean floor spreading centers, where mantle-derived basaltic material (MORB: Mid-Ocean Ridge Basalt) is upwelling. MORB derived matter is characterized by a $^{3}He/^{4}He$ ratio of about 8 times the atmospheric value (Mamyrin and Tolstikhin, 1984; Graham, 2002). The Guaymas Basin bottom water is known to be enriched in both ^{3}He and ^{4}He compared to ASW as well, since it consists of a mixture of ocean water and MORB-type hydrothermal fluids (Lupton, 1979; Berndt et al., 2016).

With the help of noble gas concentrations and isotope ratios, we aim to identify the origin of pore fluids in the sediment surrounding the recently found mound structure (Fig. 1) and to reconstruct the evolution of the active hydrothermal vent system. Based on these findings, we will discuss whether in this area only highly channelized hydrothermal fluid flow through the black smoker chimneys occurs, or whether

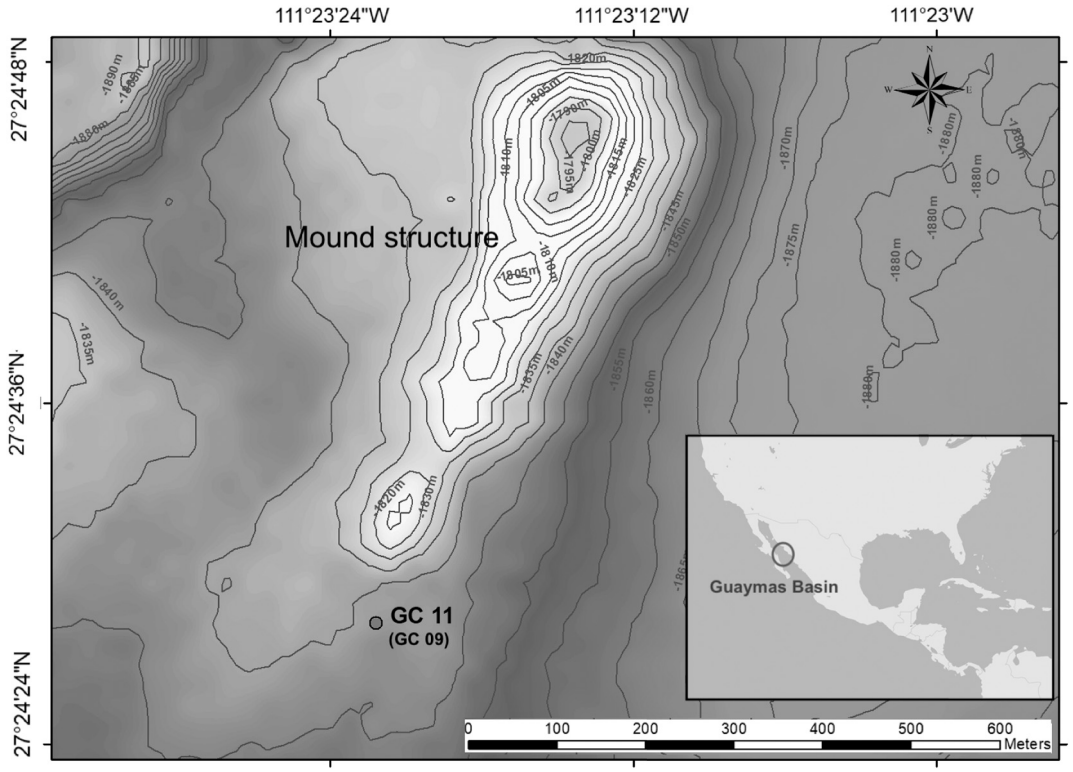

Fig. 1. Bathymetric map of the sampling location at the Northern Trough of the Guaymas Basin, Gulf of California. The sediment core GC 11 was recovered about 100 m from the southern slope of the newly discovered mound structure with several active black smokers. The second core (GC 09) was located about 15 m away from GC 11 (indicated as an identical position on this map).

hydrothermal fluids are also transported through the surrounding sediments, and emanate diffusively into the ocean as well. Since black smokers, as presented in this study, are the main source of hydrothermal venting on the EPR, it can be assumed that our findings are applicable to many other hydrothermal systems along the East Pacific Rise.

2. The GUAYMAS basin

The Guaymas Basin has been subject to many studies over the past decades, such as extensive heat flow studies (Lonsdale and Becker, 1985; Fisher and Becker, 1991), which have demonstrated that the basin is a hydrothermally active region.

The source of hydrothermal activity in the Guaymas Basin was described e.g. by Einsele et al. (1980), Kastner (1982), Gieskes et al. (1982) and Teske et al. (2019). Sills of hotmagmatic rock (derived from upwelling mantle material) intrude into cold sediments, which leads to a decrease in porosity of these sediments, and thus to an expulsion of fluids. These fluids are transported upwards through fissures and faults (Einsele et al., 1980; Lonsdale et al., 1980). The intrusion of the hot sills induces thermal alterations of the sediments (contact metamorphism), heats up the pore fluids and causes changes in their chemistry (Kastner, 1982; Teske et al., 2019), thus leading to a different chemical composition and isotope signature than ocean water. To compensate for the expelled fluids, usually ocean bottom water is entrained into the sediments further away from the vent site and transported downwards, thus causing a circulation of fluid (Kastner, 1982). The recharge areas (i.e. areas of cold ocean water inflow) are usually unknown, but could potentially be up to several tenths of kilometers away from the vent sites (Fisher et al., 2003).

Basaltic intrusions at shallow depths are usually associated with hydrothermal activity of moderate temperature (< 200 °C) and short duration (Gieskes et al., 1982). Such moderate temperature fluids were found to discharge diffusively through porous deposits in the Southern Trough of the Guaymas Basin (Lonsdale and Becker, 1985).

Venting of hydrothermal fluids at high temperatures (reported e.g. by Lonsdale et al., 1980), on the other hand, is caused by the intrusion of large-scale magma chambers at greater depths, and associated with more channelized, narrow transport pathways (Kastner, 1982; Gieskes et al., 1982). A study of the Southern Trough of the Guaymas Basin shows that highly channelized hydrothermal fluid flow occurs mainly over the central part of the underlying sill intrusion (Teske et al., 2016).

For the Northern Trough of the Guaymas Basin, so far only one highly active vent site was discovered about 1 km south-east of the rift axis showing discharge from several smokers (Berndt et al., 2016). Li and Mg data suggest that pore fluid samples taken close to the vents show only a slight imprint of a hydrothermal signature and at other sampling sites above sill intrusions located further away from the mound structure a hydrothermal imprint is missing (Geilert et al., 2018).

3. Methods

3.1. Sediment sampling and noble gas analysis

Samples were acquired during the cruise *SO241,* close to the recently discovered hydrothermal vent system south west of the rift axis of the Northern Trough of the Guaymas Basin (Berndt et al., 2016). A 5 m long gravity core ("GC11", Fig. 1) was recovered about 100 m from the southern end of the mound structure at a water depth of 1870 m for collecting samples for noble gases analysis in the sediment pore water. Another gravity core ("GC09") was recovered in close proximity (about 15 m distance) of GC11 for the determination of sediment porosity. Acquiring cores closer to the mound structure was not possible, since the hydrothermal material, which is deposited by the vents and forms the slope of the mound structure, did not allow the gravity corer to penetrate the sediment.

When the GC11 core was recovered, a sediment temperature of 68 °C was measured at the bottom of the core, while the temperature at the top was identical to that of the overlying deep ocean water temperature (3–4 °C), thus resulting in a temperature gradient of ≥12 °C/m.

A custom-made sediment press with two pistons was used to transfer the bulk sediment from the gravity core into copper tubes for later NG analysis (Brennwald et al., 2003). Starting at a position of 25 cm below the top, sediment samples were taken every 50 cm along the liner. More detailed information on this sampling method for unconsolidated sediments is given in Brennwald et al. (2003). Part of the sediments was collected in containers for further analysis, such as density and mineral composition.

The copper tube samples were prepared by high speed centrifugation which allows for separation of the sediment matrix from the pore water phase. By placing a metal clamp at the position of the sediment-water interface along the copper tube, a pure water sample was obtained in which noble gases were finally analyzed (for details see Tomonaga et al., 2011a; Tomonaga et al., 2014). Noble gas analysis was conducted at the Noble Gas Laboratory at ETH Zürich by static mass spectrometry using a well-established experimental protocol to determine concentration and isotopic ratios of noble gases in water (for details on gas separation and analysis see Beyerle et al., 2000). Using a tailored UHV-tight connection, the copper tubes containing only the pore water (separated from the sediment matrix) were coupled to the extraction vessel of the inlet of a noble gas extraction line designed especially for noble gas analysis in water (see Beyerle et al., 2000). After evacuating the extraction vessel, the copper tubes containing the pore water were opened, all gases were extracted (> 99.9 efficiency) and noble gases were analyzed following the analytical protocols to determine noble gases from water samples (see Beyerle et al., 2000).

He and Ne were separated by several cold traps capturing the rest of the extracted gases, including Ar, Kr and Xe. The He and Ne phase was purified by a series of different getters, and then volumetrically split in two fractions.

After further cleaning of the smaller fraction with a cryogenic cold trap operated at 50 K, the purified He and Ne phase was expanded and analyzed in a small tailored sector mass spectrometer trimmed for maximum linearity, but having a low mass resolution (see Beyerle et al., 2000). Simultaneously, the larger fraction was expanded to a Micromass5400 mass spectrometer with high mass resolution to determine the $^3He/^4He$ ratio of the sample. The Micromass5400 source was tuned to make the determination of the $^3He/^4He$ ratio insensitive to the total He and total gas pressure in the system.

After He and Ne measurements, Ar, Kr, and Xe were released from the cold traps, dried and transferred into a dilution reservoir. From the dried Ar-Kr-Xe phase in the reservoir a small gas aliquot was cleaned and expanded to the low-mass resolution mass spectrometer for final analysis. The dilution by about a factor of 2000 was chosen to analyze Ar, Kr and Xe simultaneously without further separation. Ar currents were measured on a Faraday cup, while Kr and Xe ions were counted on an electron multiplier (see Beyerle et al., 2000). Noble gas measurements were calibrated with a high-precision air standard. Concentrations of He, Ne, Ar and Kr have a typical over-all 1 σ-error (scaled from the deviation of the reproducibility of the air standard) of <1.5%, Xe concentrations of <2.5%, and $^3He/^4He$ ratios of <10%.

All experimental details on pore water separation from unconsolidated sediments and the performance of the applied experimental protocols to determine noble gases in water can be found in Tomonaga et al. (2011a) and Beyerle et al. (2000).

Two samples were found to be subject to experimental artefacts. One sample (at 1.75 m), which showed high helium concentrations, was most likely subjected to air contamination, as could be concluded from the helium isotope ratio. Another sample (a double aliquot at 4.25 m) showed a degassing pattern for the heavier noble gases as can be observed for an incomplete extraction of the sample. Therefore, these two samples are not further discussed.

NG concentrations in air-saturated ocean water were calculated

according to the recommended solubility data set of Kipfer et al. (2002).

3.2. Additional measurements

Sediment properties and composition were determined at GEOMAR in Kiel. Concentrations of heavy elements in the sediment, i.e. thorium, uranium, cadmium, lead and cobalt, were measured via inductively coupled plasma mass spectrometry (ICP-MS). The total density (inorganic and organic material) of the dry sediments was determined with a gas pycnometer. Additionally, X-ray diffraction measurements were conducted to determine the overall mineralogical composition of the core. This was used to estimate the inorganic (mineral) density, i.e. to eliminate the influence of organic material in the sediment on the total density. As too little material of GC11 was left un-squeezed after NG sampling, the second retrieved sediment core (GC09) was used to obtain an undisturbed porosity profile. We assume the porosity in GC09 is representative for GC11 as well, since they are equally close to the mound structure and have a similar sediment composition.

4. Results

4.1. Density and heavy elements in the sediment matrix

The total (inorganic and organic) density of the sediment matrix along the core increases with depth, from 2.2 g/cm^3 at the top to about 2.5 g/cm^3 at the bottom (Fig. 2a). At a depth of about 4 m, a layer of especially high density with values of 2.9 g/cm^3 is found. In the inorganic (mineral) density profile, this layer is even more prominent (Fig. 2a). The average density of minerals in the sediment matrix is about 3.2 g/cm^3, whereas in the layer at 4 m depth, mineral densities as high as 3.9 g/cm^3 are observed. The porosity decreases with depth, declining from values of 0.8 at the top to 0.7 at the bottom and shows an overall high scatter (Fig. 2b).

The high-density layer (H-DL) at 4 m depth also stands out with regards to the abundances of heavy elements (Fig. 2c and d). While cobalt and thorium decrease by 80% (with respect to their respective average concentrations along the profile) in this layer, the concentrations of cadmium and lead increase by a factor of more than 10. High lead concentrations are often reported to be found in hydrothermal

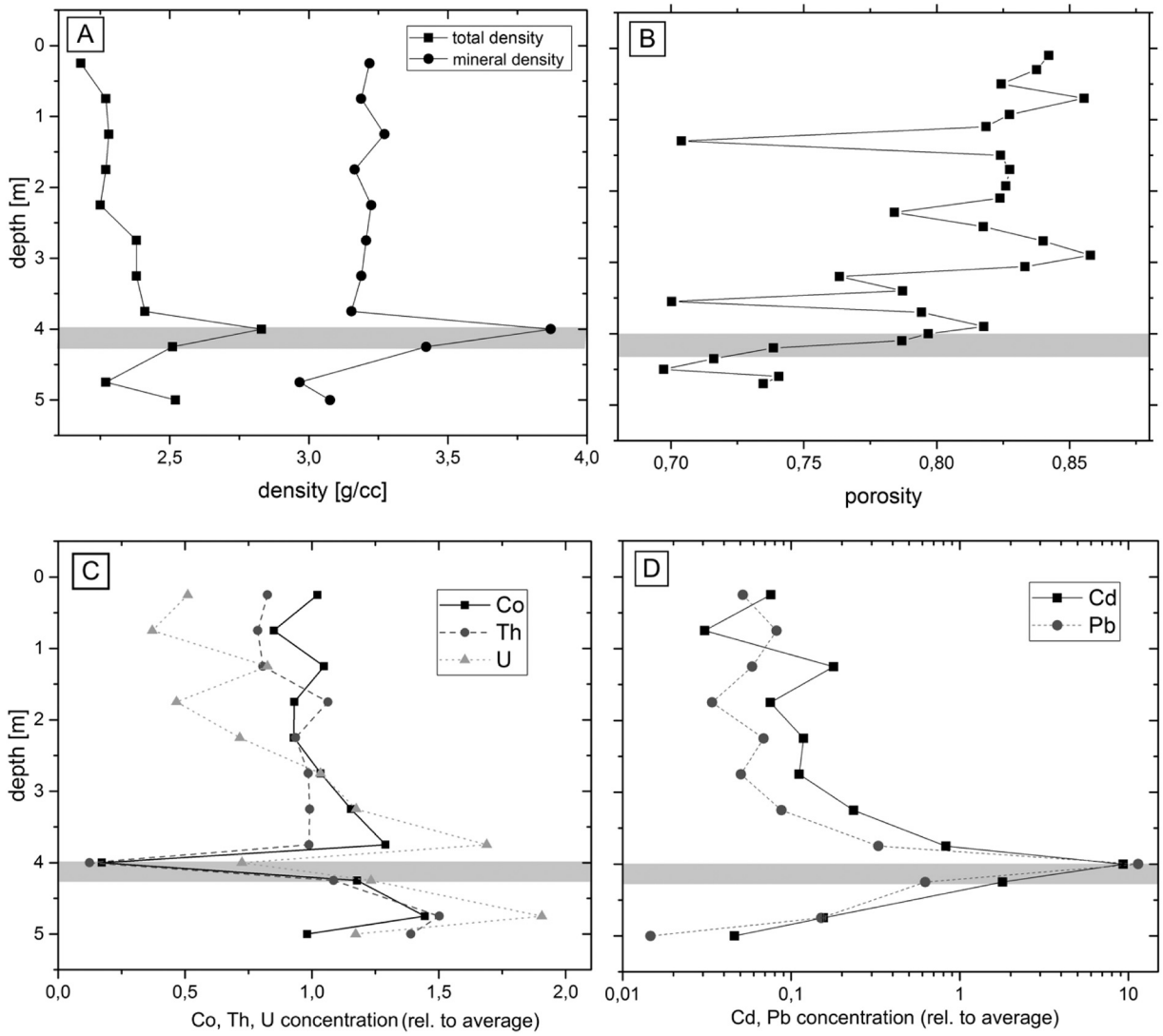

Fig. 2. a) Density and porosity of dry sediments: total density (organic and inorganic material) obtained by a pycnometer, and scaled density of minerals from XRD measurements. b) Porosity taken from neighbouring core (GC09, about 15 m distance). The grey-shaded area indicates the high-density layer at 4 m depth. c) and d) Concentrations of various heavy metals with depth (uncertainties smaller than symbol size). Concentrations are plotted relative to the average value of the respective metal across depth. c) cobalt, thorium and uranium, whose concentrations decrease in the dense layer. d) cadmiun and lead concentrations, which are strongly enriched in the dense layer (note logarithmic scale).

deposits (Peter and Scott, 1988; Tivey, 2007). Overall, the uranium concentration tends to increase with sediment depth. For detailed results of sediment properties and heavy element measurements, see Horstmann et al. (2020).

4.2. Neon, argon, krypton, xenon dissolved in the pore fluids

The concentrations of the heavier noble gases in the pore fluids of the sampled sediments (Fig. 3) agree reasonably well with air saturated water (ASW) concentrations at ocean water temperatures (about 3–4 °C) and salinities (about 34–35‰). The concentrations remain constant throughout the entire pore water profile, and there is no trend with depth, therefore they can be assumed to be solely of atmospheric origin. This leads to the conclusion that only ocean water, and no additional hydrothermal fluid can be found in the sediment pore space. All noble gas concentrations (He, Ne, Ar, Kr and Xe) and the $^3He/^4He$ isotope ratios and the according errors are listed in Table 1. For detailed results of NG measurements, see Horstmann et al. (2020).

4.3. Helium dissolved in the pore fluids

The total He concentrations in the sediment core show a generally larger variability than the concentrations of the heavier noble gases. Considering this large variability in the data, the He concentrations do not show an obvious trend with depth (Fig. 4), particularly if the variability of duplicate aliquots from the same depth (see samples at 2.25 m) is taken into account.

In contrast to Ne-Xe, the He concentrations exceed the atmospheric equilibrium concentration by 10–15%. The He concentrations agree with those of Guaymas Basin bottom water, which were reported to show a He excess of up to 12.4% (Lupton, 1979). Again, this leads to the conclusion that the He concentrations of the pore water in the sediment column are also consistent with those of the overlying water body.

The $^3He/^4He$ ratios, however, show a different pattern than the noble gas concentrations (Fig. 5). Above 2.25 m and below 4 m, the ratios are in a range of 1.6 to 1.8 with respect to the ASW ratio. Since Lupton (1979) reported enriched $^3He/^4He$ ratios in the deep water of the Guaymas Basin exceeding the ASW ratio by up to 70%, we again assume that the ratios observed in these parts of the sediment core are indicative for entrapped Guaymas Basin bottom water.

However, between 2.25 m and 4 m, a zone with an even higher

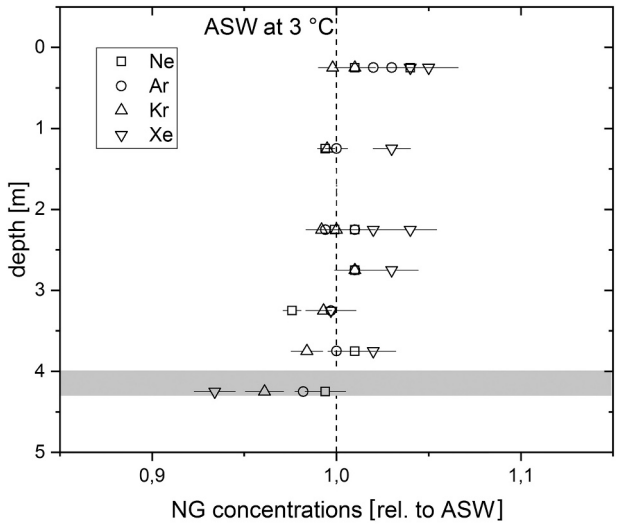

Fig. 3. Concentrations of noble gases (except helium), relative to air-saturated water vs. depth in sediment core. The dashed line represents the atmospheric equilibrium concentration (ASW) of each gas at 3 °C and a salinity of 34‰. The grey area marks the high-density layer. Error bars represent uncertainties of 1 σ.

Table 1
Overview of all noble gas concentrations and He isotope ratios, normalized to the respective ASW concentrations ($T = 3$ °C, S = 35‰) and with absolute errors. Ne-Xe are of atmospheric origin, thus the values are closer to 1 than for He, which is partly of mantle origin. In the bottom row, the absolute values of ASW concentration for each gas species are given.

Depth (m)		He		Ne		Ar		Kr		Xe		^{3}He		/ ^{4}He
0,25	1103	+/−	0,018	1040	+/−	0,005	1030	+/−	0,006	1010	+/−	0,007	1050	+/−	0,016	1457	+/−	0,111
0,25	1124	+/−	0,005	1010	+/−	0,011	1020	+/−	0,005	0,998	+/−	0,008	1040	+/−	0,013	1782	+/−	0,136
1,25	1099	+/−	0,005	0,994	+/−	0,004	1000	+/−	0,006	0,995	+/−	0,004	1030	+/−	0,010	1558	+/−	0,103
2,25	1101	+/−	0,006	0,999	+/−	0,011	0,994	+/−	0,005	1000	+/−	0,008	1040	+/−	0,014	1754	+/−	0,133
2,25	1160	+/−	0,006	1010	+/−	0,011	1010	+/−	0,005	0,992	+/−	0,009	1020	+/−	0,012	1857	+/−	0,141
2,75	1134	+/−	0,005	1010	+/−	0,011	1010	+/−	0,005	1010	+/−	0,008	1030	+/−	0,014	2383	+/−	0,181
3,25	1132	+/−	0,014	0,976	+/−	0,005	0,997	+/−	0,006	0,993	+/−	0,004	0,997	+/−	0,014	2478	+/−	0,189
3,75	1155	+/−	0,006	1010	+/−	0,011	1000	+/−	0,005	0,984	+/−	0,009	1020	+/−	0,012	2073	+/−	0,158
4,25	1137	+/−	0,004	0,994	+/−	0,011	0,982	+/−	0,005	0,961	+/−	0,010	0,934	+/−	0,011	1820	+/−	0,138
ASW conc. (ccSTP/g)		3,92E-08		1,72E-07			3,53E-04			8,58E-08			1,26E-08			1,36E-06		

The given experimental errors of NG concentrations account for the overall error of the experimental procedure, and also account for the reproducibility of the air calibration standard (≤ 1.5%). The typical error of $^3He/^4He$ ratios is in the order of about 10%, which is dominated by the counting statistics of the very low ^{3}He abundance of the samples.

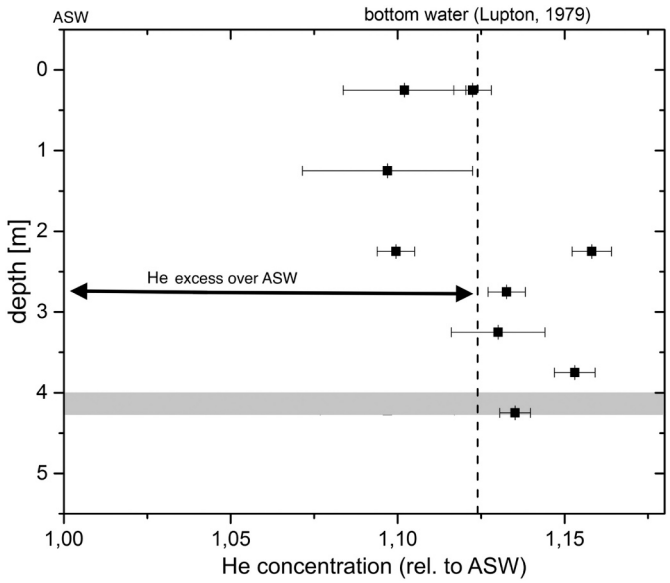

Fig. 4. Total helium concentration relative to ASW with depth. The dashed line represents bottom water concentrations of the Guaymas Basin found by Lupton (1979). The grey area marks the high-density layer. Error bars represent uncertainties of 1 σ.

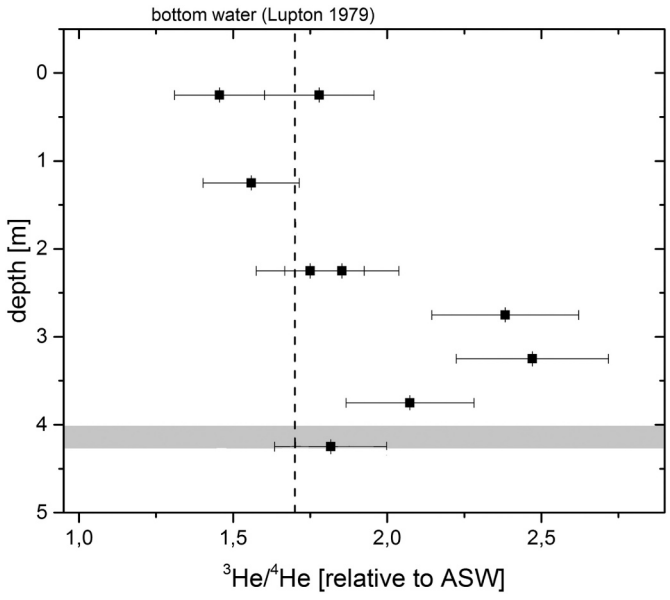

Fig. 5. ^{3}He/^{4}He ratio relative to ASW with depth. The dashed line represents bottom water ratios in the Guaymas Basin found by Lupton (1979). The grey area marks the high-density layer. Error bars represent uncertainties of 1 σ.

^{3}He/^{4}He ratio than in the remainder of the profile can be observed, with a maximum at approximately 3 m, i.e. slightly above the H-DL. The ^{3}He/^{4}He ratio at this depth exceeds the ASW ratio by a factor of 2.5. Such high ratios have not been reported in today's deep bottom water body of the Guaymas Basin.

5. Discussion

5.1. Pore water origin and hydrothermal fluid transport

The NG concentrations along the sediment profile are consistent with the Guaymas Basin bottom water concentrations, and there is no concentration gradient with depth. In particular, the helium concentration makes the case that there is no evidence of an additional hydrothermal fluid component in the pore space, as this would result in helium concentrations higher than the concentrations observed in the Guaymas Basin bottom water. We conclude that there is virtually no (diffusive) hydrothermal fluid transport through the sediments surrounding the vent system, as diffusive fluid transport from the deep source through the surrounding sediments would result in a continuous concentration gradient throughout the sediment column (e.g. Tomonaga et al., 2011b; Tomonaga et al., 2014). In addition, the concentrations of Ne-Xe in the pore water are in close agreement with ASW concentrations. This observation is contrasting findings in typical hydrothermal fluids where NG concentrations were found to be strongly depleted (20–30%) in response to subsurface boiling (Winckler et al., 2000). This indicates that the pore fluids do not contain a large hydrothermal component.

Thus, we interpret the NG concentration profiles in pore water as direct evidence that fluid transport from the hot hydrothermal reaction zone (source) to the sediment surface at the investigated black smoker site is indeed limited to narrow pathways beneath the chimneys. This implies that the strong temperature gradient observed in the sediment core is not caused by hydrothermal fluid infiltration from below, but is only attributed to heat conduction, as was already proposed by Geilert et al. (2018).

5.2. Evolution of the vent system

The distinct layer (H-DL) at 4 m depth, which was also found in other sediment cores in this region during the *SO241* expedition (see cruise report RV SO241: Berndt et al., 2015), consists of hydrothermal deposits, while above this layer mostly organic-rich hemipelagic sediments are found (Berndt et al., 2016). The high density in this layer hints to a time during which a large amount of hydrothermal material was deposited rapidly by the vent system. Thus, we conclude the vent system had a more active time period in the past. During the following less active phase, lasting until the present day, the sedimentation of regular pelagic sediments dominated the overall sediment deposition.

Berndt et al. (2016) report that the H-DL was likely deposited when the mound structure was initially formed. According to sedimentation rates in the hydrothermal vent field, the depth of the layer corresponds to a sediment age of 5–6 ka (Berndt et al., 2016), which would represent the minimum age of the vent field. The idea of an early more active stage of hydrothermal vent systems is further supported by studies modeling the life time of such systems (Bani-Hassan, 2012; Iyer et al., 2017). The authors report rigorous venting in the initial phase of evolution, which subsequently decreases rapidly.

The high ^{3}He/^{4}He ratio at 3 m depth (Fig. 5) is likely to be associated with the HD-L at 4 m, i.e. the isotopically light He was incorporated into the sediment column about 5–6 kyr ago. The reason for this distance of about 1 m can be explained by the compaction flux: As the sediment matrix has been compacted over time, the sediment layer and the associated pore water phase have slowly moved apart (for details on the compaction flux, see Imboden (1975) and Strassmann et al. (2005).

Since we can conclude from the absolute NG concentrations that we only find Guaymas Basin bottom water in the sediment pore space (see previous subsection), this means in turn that about 5–6 kyr ago the Guaymas Basin bottom water must have had a higher ^{3}He/^{4}He signature. Thus, we assume that during the early stages of the vent system, fluids with a higher ^{3}He/^{4}He ratio were emitted by the smokers. As the ^{3}He/^{4}He ratios we observe at around 3 m do not match the ratio of the current Guaymas Basin bottom water, the signal must have been preserved in the sediment, and diffusive transport must be strongly suppressed. The most likely reason for reduced exchange in the pore water is the realignment of minerals during compaction, leading to decreased viscosity and a disconnected pore space (Brennwald et al., 2013).

To make the case that the high ^{3}He/^{4}He signature cannot be

explained by present-day hydrothermal fluids being transported through the sediments, we show the mixing line of ocean water (ASW) and hydrothermal fluids with the present-day MORB signature (Fig. 6). In this plot, excess ^{3}He and ^{4}He, normalized to Ne are shown (see Lupton, 1979):

$$\Delta \mathrm{iHe} \Big/ \mathrm{Ne} = \left(\frac{\left[{}^{i}He\right]_{meas} \Big/ \left[{}^{i}He\right]_{ASW}}{[Ne]_{meas} / [Ne]_{ASW}} - 1 \right) \times 100\%$$

The data from Lupton (1979) depict the present-day bottom water signatures of the Guaymas Basin. The data taken from Berndt et al. (2016) represent background bottom water samples, water samples taken within the vent field, and one fluid sample taken directly from the water column above one of the venting black smokers with extremely high Δ^{i}He/Ne. This highly enriched sample allows us to characterize the helium signature of the fluids emanating from the smokers today, although even this sample is to some extent already diluted with ambient sea water.

Fitting a line through these water sample data, we obtain the recent mixing trend between ASW and MORB-derived fluids in the Guaymas Basin. Note that even though the plotted mixing line spans several orders of magnitude in Δ^3He/Ne and Δ^4He/Ne, all the water sample data lie very closely on the mixing line. Sediment pore fluid data presented in this study lie on the lower left of the mixing trend, representing Guaymas Basin bottom water (i.e. ocean water with a slight hydrothermal signature). Like in the case of the water samples, the majority of the sediment data lie very close to the mixing line, with the exception of the three samples from the middle of the core which represent the peak in the ^{3}He/^{4}He profile (Fig. 5). The isotopic composition of these three samples thus cannot be explained by mixing between ASW and fluids emitted by the vent system today. This means there must have been a time in the past during which fluids with a higher ^{3}He/^{4}He ratio were emitted by the vents and embedded into the sediment column as ambient bottom water.

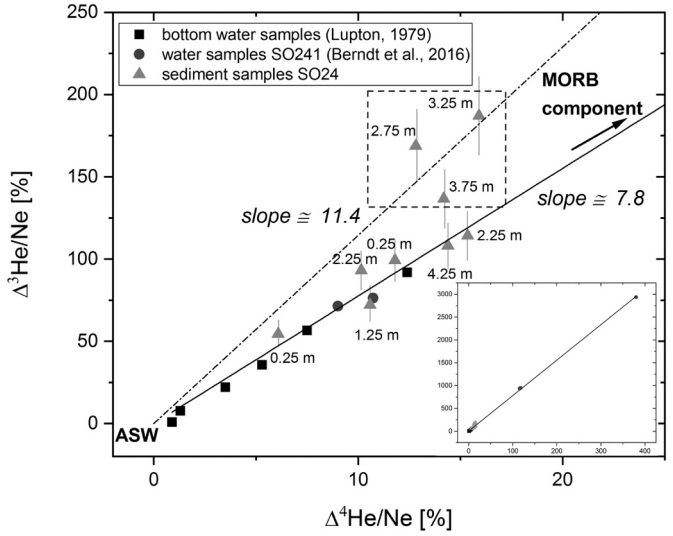

Fig. 6. Δ^3He/Ne vs. Δ^4He/Ne ("excess helium", for definition see section 5.2). The large graph shows a close-up section of the data discussed in this study, while the small graph in the lower right corner shows the values on a larger scale. The black line is a fit to the data of both Lupton (1979) and Berndt et al. (2016), and represents a mixing trend between ASW and the present day MORB component. The dashed square highlights three sediment pore water samples which do not lie on the mixing line. The dashed line is a fit to these three sediment pore water samples, representing injection of fluids with a higher ^{3}He/^{4}He ratio than today. We note that within the error bars the helium composition of the samples between 2.75 m and 3.75 m cannot be explained by binary mixing of ASW and hydrothermal component currently observed in the Guaymas Basin.

In Fig. 6, the slope of the line fitted through the data can be used to determine the ^{3}He/^{4}He ratio of the hydrothermal fluids injected into the Guaymas Basin (To be compatible with earlier work, we follow the interpretative scheme of Lupton (1979): a line with a slope of 1 would represent injection of helium with a ^{3}He/^{4}He ratio of 1 R_A (^{3}He/^{4}He ratio of atmospheric air: $1.384 \cdot 10^{-6}$, see Clarke et al., 1976). The helium data from the water samples and most of the presented sediment samples lie on a slope of 7.8, which represents injection of helium with a ^{3}He/^{4}He ratio of 7.8 R_A (a value typical for MORB), as it occurs in the Guaymas Basin today (Lupton, 1979; Berndt et al., 2016). A mixing line of ASW and the three porewater samples with high ^{3}He values (derived from the H-DL) indicates that during the initial activity of the vent field, hydrothermal fluids with a ^{3}He/^{4}He ratio of 11.4 R_A were injected into the Guaymas Basin (Fig. 6).

Due to the short lifetime of the smoker system of a few thousand years, we speculate that the higher ^{3}He/^{4}He ratio during the early stages may be related to a slightly different fluid transport at that time. During this early active stage, a free gas phase may have formed in response to the increased activity of the vent system. Such a phase partitioning would fractionate helium isotopes in favor of the lighter, more mobile isotope into the gas phase, as has been observed in hydrothermal systems before (e.g. Barry et al., 2013; Barry et al., 2020). If these ^{3}He-rich fluids were emitted by the smokers (either as a free gas phase or dissolved gas) during the early evolutionary stages of the vent system, this would have led to increased ^{3}He/^{4}He ratios in the bottom water, and thus in the pore fluids entrapped in the growing sediment column.

Variation in vent fluid composition in the Guaymas Basin has already been suggested by Peter and Scott (1988), who report that the salinity of fluid inclusions found in chimney deposits cannot always be explained by mixing of present-day vent fluids and ocean water.

6. Conclusions

To obtain a conceptual model to reasonably estimate the amount of fluids and gases being released by a certain hydrothermal vent system throughout its lifetime, it is necessary to know the typical fluid transport pathways for this type of vent system (i.e. narrow and focused, or diffuse and wide-spread). For systems with very focused transport, only the output of individual vents contributes significantly to the fluid emissions in the area, and a model of point-like injection of hydrothermal fluids into the ocean can be used. In this case, it is possible to estimate the fluid output of a whole hydrothermally active region from the number of vents in it and the output of a single vent. In systems characterized by diffuse, widespread fluid emanation, the sediment surrounding the vents contribute to the hydrothermal fluid output of the area as well, making the estimation of fluid emission more challenging.

Our findings show that the pore space of the sediments even in close vicinity to the vent site contains only Guaymas Basin bottom water, and higher concentrations of hydrothermal fluids are only found in the water column directly above the vents (Berndt et al., 2016). This implies that for the studied hydrothermal vent site, the main input of hydrothermal fluids into the ocean water originates from the smoker chimneys. Thus, when estimating or modeling the overall output of fluids or of a specific gas, only the contribution of the black smokers has to be considered, and additional diffuse output by diffusive transport from the surrounding sediments can be neglected.

Funding sources

This work was funded and supported by the Swiss National Science Foundation (project: 'Noble gases trapped in the pore fluids of aquatic sediments as environmental tracers', grants: 200021_162447 & 200021_162447 / 2), the Swiss Federal Institute of Aquatic Science and Technology, and the GEOMAR Helmholtz Centre for Ocean Research Kiel.

Declaration of Competing Interest

The authors declare that they have no known competing financial interests or personal relationships that could have appeared to influence the work reported in this paper.

Acknowledgements

We acknowledge the Noble Gas Laboratory at ETH Zürich, particularly Dr. Colin Maden for their technical advice and support for the noble gas analysis of pore waters. We acknowledge the valuable input of two anonymous reviewers to an earlier version of the manuscript, which significantly helped to improve our work.

References

Bani-Hassan, N., 2012. Numerical Modeling of Submarine Hydrothermal Fluid Flow. Dr. Diss. Christian-Albrechts-Universität Kiel, Germany.

Barry, P.H., Hilton, D.R., Fischer, T.P., de Moor, J.M., Mangasini, F., Ramirez, C., 2013. Helium and carbon isotope systematics of cold "mazuku" CO2vents and hydrothermal gases and fluids from Rungwe Volcanic Province, southern Tanzania. Chem. Geol. 339, 141–156. https://doi.org/10.1016/j.chemgeo.2012.07.003.

Barry, P.H., Negrete-Aranda, R., Spelz, R.M., Seltzer, A.M., Bekaert, D.V., Virrueta, C., Kulongoski, J.T., 2020. Volatile sources, sinks and pathways: a helium-carbon isotope study of Baja California fluids and gases. Chem. Geol. 550, 119722. https://doi.org/10.1016/j.chemgeo.2020.119722.

Berndt, C., Hensen, C., Muff, S., Karstens, J., Schmidt, M., Liebetrau, V., Kipfer, R., Lever, M., Böttner, C., Doll, M., Sarkar, S., Geilert, S., 2015. RV SONNE 241 Cruise Report / Fahrtbericht, Manzanillo, 23.6.2015 – Guayaquil, 24.7.2015: SO241 - MAKS: Magmatism induced carbon escape from marine sediments as a climate driver – Guaymas Basin, Gulf of California. https://doi.org/10.3289/CR_S241.

Berndt, C., Hensen, C., Mortera-Gutierrez, C., Sarkar, S., Geilert, S., Schmidt, M., Liebetrau, V., Kipfer, R., Scholz, F., Doll, M., Muff, S., Karstens, J., Planke, S., Petersen, S., Bottner, C., Chi, W.C., Moser, M., Behrendt, R., Fiskal, A., Lever, Mark A., Su, C.C., Deng, L., Brennwald, M., Lizarralde, S.D., 2016. Rifting under steam—how rift magmatism triggers methane venting from sedimentary basins. Geology 44 (9), 767–770. https://doi.org/10.1130/g38049.1.

Beyerle, U., Aeschbach-Hertig, W., Imboden, D., Baur, H., Graf, T., Kipfer, R., 2000. A mass, spectrometric system for the analysis of noble gases and tritium from water samples. Environ. Sci. Technol. 34, 2042–2050. https://doi.org/10.1021/es990840h.

Brennwald, M.S., Hofer, M., Peeters, F., Aeschbach-Hertig, W., Strassmann, K., Kipfer, R., 2003. Analysis of dissolved noble gases in the porewater of lacustrine sediments. Limnol. Oceanogr. Methods 1 (1), 51–62. https://doi.org/10.4319/lom.2003.1.51.

Brennwald, M.S., Vogel, N., Scheidegger, Y., Tomonaga, Y., Livingstone, D.M., Kipfer, R., 2013. Noble gases as Environmental tracers in sediment porewaters and stalagmite fluid inclusions. Noble Gases Geochem. Tracers 123–153. https://doi.org/10.1007/978-3-642-28836-4_6.

Clarke, W.B., Jenkins, W.J., Top, Z., 1976. Determination of tritium by mass spectrometric measurement of 3He. Int. J. Appl. Radiat. Isot. 27, 515–522. https://doi.org/10.1016/0020-708X(76)90082-X.

Corliss, J.B., Dymond, J., Gordon, L.I., Edmond, J.M., von Herzen, R.P., Ballard, R.D., Green, K., Williams, D., Bainbridge, A., Crane, K., van Andel, T.H., 1979. Submarine thermal springs on the Galapagos Rift. Science 20, 1073–1083. https://doi.org/10.1126/science.203.4385.1073.

Einsele, G., Gieskes, J.M., Curray, J., Moore, D.M., Aguayo, E., Aubry, M.P., Fornari, D., Guerrero, J., Kastner, M., Kelts, K., Lyle, M., Matoba, Y., Molina-Cruz, A., Niemitz, J., Rueda, J., Saunders, A., Schrader, H., Simoneit, B., Vacquier, V., 1980. Intrusion of basaltic sills into highly porous sediments, and resulting hydrothermal activity. Nature 283, 441–445. https://doi.org/10.1038/283441a0.

Fisher, A.T., Becker, K., 1991. Heat flow, hydrothermal circulation and basalt intrusions in the Guaymas Basin, Gulf of California. Earth Planet. Sci. Lett. 103, 84–99. https://doi.org/10.1016/0012-821X(91)90152-8.

Fisher, A.T., Davis, E.E., Hutnak, M., Spiess, V., Zühlsdorff, L., Cherkaoui, A., Christiansen, L., Edwards, K., Macdonald, R., Villinger, H., Mottl, M., Wheat, C., Becker, K., 2003. Hydrothermal recharge and discharge across 50 km guided by seamounts on a young ridge flank. Nature 421, 618–621. https://doi.org/10.1038/nature01352.

Geilert, S., Hensen, C., Schmidt, M., Liebetrau, V., Scholz, F., Doll, M., Deng, L., Fiskal, A., Lever, M., Su, C., Schloemer, S., Sarkar, S., Thiel, V., Berndt, C., 2018. On the formation of hydrothermal vents and cold seeps in the Guaymas Basin, Gulf of California. Biogeosciences 15, 5715–5731. https://doi.org/10.5194/bg-15-5715-2018.

Gieskes, J.M., Kastner, M., Einsele, G., Kelts, K., Niemitz, J., 1982. Hydrothermal activity in the Guaymas Basin, Gulf of California: a Synthesis. In: Curray, J.R., Moore, D.G. (Eds.), Initial Reports of the Deep Sea Drilling Project, 64. U.S. Government Printing Office. https://doi.org/10.2973/dsdp.proc.64.155.1982.

Goldfarb, M.S., Converse, D.R., Holland, H.D., Edmond, J.M., 1983. The genesis of hot spring deposits on the East Pacific rise, 21°N. In: The Kuroko and Related Volcanogenic Massive Sulfide Deposits. https://doi.org/10.5382/Mono.05.11.

Graham, D.W., 2002. Noble gas isotope geochemistry of mid-ocean ridge and ocean island basalts: characterization of mantle source reservoirs. Rev. Mineral. Geochem. 47 (1), 247–317. https://doi.org/10.2138/rmg.2002.47.8.

Grathwohl, P., 1998. Diffusion in Natural Porous Media, Topics in Environmental Fluid Mechanics. Kluwer Academic Publishers, Boston.

Haymon, R.M., 1983. Growth history of hydrothermal black smoker chimneys. Nature 301 (5902), 695–698. https://doi.org/10.1038/301695a0.

Horseman, S., Higgo, J., Alexander, J., Harrington, J., 1996. Water, gas and solute movement through argillaceous media. In: Technical Report CC-96/1. OECD Nuclear Energy Agency, France.

Horstmann, E., Kipfer, R., Schmidt, M., Liebetrau, V., 2020. SO241 cuise 2015, Guaymas Basin, noble gas data and sediment properties. Mendeley Data 1. 10.17632/9x4b7mkvw9.1.

Imboden, D.M., 1975. Interstitial transport of solutes in non-steady state accumulating and compacting sediments. Earth Planet. Sci. Lett. 27 (2), 221–228. https://doi.org/10.1016/0012-821x(75)90033-3.

Iyer, K., Schmid, D.W., Planke, S., Millett, J., 2017. Modelling hydrothermal venting in volcanic sedimentary basins: Impact on hydrocarbon maturation and paleoclimate. Earth Planet. Sci. Lett. 467, 30–42. https://doi.org/10.1016/j.epsl.2017.03.023.

Kastner, M., 1982. Evidence for two distinct hydrothermal systems in the guaymas basin. In: Curray, J.R., Moore, D.G. (Eds.), Initial Reports of the Deep Sea Drilling Project, 64. U.S. Government Printing Office. https://doi.org/10.2973/dsdp.proc.64.154.1982.

Kipfer, R., Aeschbach-Hertig, W., Peeters, F., Stute, M., 2002. 14. Noble gases in lakes and ground waters. Noble Gases 615–700. https://doi.org/10.1515/9781501509056-016.

Lonsdale, P., Becker, K., 1985. Hydrothermal plumes, hot springs, and conductive heat flow in the Southern Trough of Guaymas Basin. Earth Planet. Sci. Lett. 73, 211–225. https://doi.org/10.1016/0012-821X(85)90070-6.

Lonsdale, P.F., Bischoff, J.L., Burns, V.M., Kastner, M., Sweeney, R.E., 1980. A high-temperature hydrothermal deposit on the seabed at a gulf of California spreading center. Earth Planet. Sci. Lett. 49, 8–20. https://doi.org/10.1016/0012-821X(80)90144-2.

Lupton, J.E., 1979. Helium-3 in the Guaymas basin: evidence for injection of mantle volatiles in the Gulf of California. J. Geophys. Res. 84, 7446–7452. https://doi.org/10.1029/JB084iB13p07446.

Mamyrin, B.A., Tolstikhin, I.N., 1984. Helium Isotopes in Nature, , 1st ed.3. Elsevier, Netherlands.

Peter, J.M., Scott, S.D., 1988. Mineralogy, composition, and fluid-inclusion microthermometry of seafloor hydrothermal deposits in the Southern Trough of Guaymas Basin, Gulf of California. Can. Mineral. 26 (3), 567–587.

Pitre, F., Pinti, D.L., 2010. Noble gas enrichments in porewater of estuarine sediments and their effect on the estimation of net denitrification rates. Geochim. Cosmochim. Acta 74, 531–539. https://doi.org/10.1016/j.gca.2009.10.004.

Renkin, E.M., 1954. Filtration, diffusion, and molecular sieving through porous cellulose membranes. J. General Physiol. 38, 225–243.

Rona, P.A., 1984. Hydrothermal mineralization at seafloor spreading centers. Earth Sci. Rev. 20 (1), 1–104. https://doi.org/10.1016/0012-8252(84)90080-1.

Schwarzenbach, R.P., Gschwend, P.M., Imboden, D.M., 2003. Environmental Organic Chemistry, 2nd edn. Wiley, New York.

Strassmann, K.M., Brennwald, M.S., Peeters, F., Kipfer, R., 2005. Dissolved noble gases in the porewater of lacustrine sediments as palaeolimnological proxies. Geochim. Cosmochim. Acta 69 (7), 1665–1674. https://doi.org/10.1016/j.gca.2004.07.037.

Svensen, H., Planke, S., Malthe-Sørenssen, A., Jamtveit, B., Myklebust, R., Eidem, T.R., Rey, S.S., 2004. Release of methane from a volcanic basin as a mechanism for initial Eocene global warming. Nature 429 (6991), 542–545. https://doi.org/10.1038/nature02566.

Talwani, M., Windisch, C.C., Langseth, M.G., 1971. Reykjanes ridge crest: a detailed geophysical study. J. Geophys. Res. 76, 473–517. https://doi.org/10.1029/JB076i002p00473.

Teske, A., De Beer, D., McKay, L.J., Tivey, M.K., Biddle, J.F., Hoer, D., Lloyd, K., Lever, M., Røy, H., Albert, D., Mendlovitz, H., MacGregor, B.J., 2016. The Guaymas Basin hiking guide to hydrothermal mounds, chimneys, and microbial mats: complex seafloor expressions of subsurface hydrothermal circulation. Front. Microbiol. 7 https://doi.org/10.3389/fmicb.2016.00075.

Teske, A., McKay, L.J., Ravelo, A.C., Aiello, I., Mortera, C., Nunez-Useche, F., Canet, C., Chanton, J., Brunner, B., Hensen, C., Ramírez, G., Sibert, R., Turner, T., White, D., Chambers, C., Buckley, A., Joye, S., Soule, S., Lizarralde, D., 2019. Characteristics and Evolution of sill-driven off-axis hydrothermalism in Guaymas Basin – the Ringvent site. Sci. Rep. 9 https://doi.org/10.1038/s41598-019-50200-5.

Tivey, M., 2007. Generation of seafloor hydrothermal vent fluids and associated mineral deposits. Oceanography 20 (1), 0–65. https://doi.org/10.5670/oceanog.2007.80.

Tomonaga, Y., Brennwald, M.S., Kipfer, R., 2011a. An improved method for the analysis of dissolved noble gases in the porewater of unconsolidated sediments. Limnol. Oceanogr. Methods 9, 42–49. https://doi.org/10.4319/lom.2011.9.42.

Tomonaga, Y., Brennwald, M.S., Kipfer, R., 2011b. Spatial distribution and flux of terrigenic he dissolved in the sediment pore water of Lake Van (Turkey). Geochim. Cosmochim. Acta 75, 2848–2864. https://doi.org/10.1016/j.gca.2011.02.038.

Tomonaga, Y., Brennwald, M.S., Meydan, A.F., Kipfer, R., 2014. Noble gases in the sediments of Lake Van - solute transport and palaeoenvironmental reconstruction. Quat. Sci. Rev. 104, 117–126. https://doi.org/10.1016/j.quascirev.2014.09.005.

Tomonaga, Y., Brennwald, M.S., Kipfer, R., 2015. Attenuation of diffusive noble-gas transport in laminated sediments of the Stockholm Archipelago. Limnol. Oceanogr. 60 (2), 497–511. https://doi.org/10.1002/lno.10045.

Winckler, G., Kipfer, R., Aeschbach-Hertig, W., Botz, R., Schmidt, M., Schuler, S., Bayer, R., 2000. Sub Sea floor boiling of Red Sea brines: new indication from noble

gas data. Geochim. Cosmochim. Acta 64 (9), 1567–1575. https://doi.org/10.1016/S0016-7037(99)00441-X.